Applicability of Friction Stir Welding (FSW) to Steels and Properties of the Welds[†]

MATSUSHITA Muneo[*1]   KITANI Yasushi[*2]   IKEDA Rinsei[*3]

Abstract:

Applicability of friction stir welding (FSW) to steels was studied with respect to the tensile strength and thickness of base metal. Using the advanced high strength steel sheets with tensile strength grade between 590 and 1 180 N • mm^{-2} and thickness of 1.6 mm for automotive applications, the appropriate parameter windows for tested steels were investigated. The result showed that the higher the tensile strength of base metal was, the narrower the parameter window became. The investigation of weld joint properties verified that the tensile strength of weld joint was as high as that of the base metal up to 980 N • mm^{-2} grade. Using the structural steel plates with thickness of 12 mm and tensile strength grade of 400 N • mm^{-2}, it was verified that the appropriate parameter existed to produce sound welds, and the investigation of mechanical properties of weld indicated that the toughness within the stir zone showed the variation, conceivably attributed to the inhomogeneous microstructure evolution.
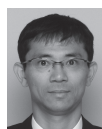
1. Introduction

Friction stir welding (FSW)[1] is a joining method which makes it possible to obtain low strain, high quality welds without fusion during welding. While FSW has been studied widely as a technology for aluminum alloys, magnesium alloys, and other low melting point metal materials which are difficult to join by conventional welding methods, and practical application is progressing[2, 3], hitherto little progress has been made in application of FSW to steel materials due to the problem of durability of the FWS tool. However, with the development of FSW tools that can withstand joining of ferrous materials, FSW is expected to offer a solution in cases where weldability, welded joint properties, or welding cost is a problem with conventional welding methods. Several reports have already been published on FSW of IF (interstitial free) steel[4], carbon steel[5–15], and stainless steel[16–20]. In particular, Fujii et al.[9–11] studied FSW of several grades of carbon steel with different carbon contents, and reported in detail on the relationship between the weld microstructure and the thermal history during welding, including the peak temperature, cooling rate, etc., which change depending on the welding conditions, and the carbon content of the steel.

For FSW to reach practical application as a joining method for steel materials, in the future, it will be necessary to obtain the required welding efficiency and cost applicability while also satisfying the required joint properties. However, these issues have not been adequately studied so far.

Therefore, in this research, FSW was performed using advanced high strength steel sheets for automotive applications with tensile strength grades between 590 and 1 180 N • mm^{-2} with the aim of applying FSW to high tensile strength steel sheets. The appropriate parameter window within which defect-free joints can be obtained was verified, and the microstructure and tensile properties of the joints produced by using the obtained parameters were investigated. FSW was also performed with structural steel plates with a thickness of 12 mm with the aim of applying FSW to plates for large-scale structures. The existence of appropriate parameters which make it possible to obtain sound joints was confirmed, and the microstructure and mechanical proper-

[*2] Dr. Eng.,
Senior Researcher Deputy General Manager,
Joining & Strength Res. Dept.,
Steel Res. Lab.,
JFE Steel

[*1] Ph. D.,
Senior Researcher Manager,
Joining & Strength Res. Dept.,
Steel Res. Lab.,
JFE Steel

[*3] Dr. Eng.,
Senior Researcher General Manager,
Joining & Strength Res. Dept.,
Steel Res. Lab.,
JFE Steel

ties of the obtained joints such as tensile properties and Charpy toughness were evaluated.

2. FSW of High Strength Steel Sheets for Automotive Applications

2.1 Experimental Method

Automotive cold-rolled steel sheets of four tensile strength grades from 590 to 1 180 N • mm^{-2} were used as materials for FSW tests. In all cases, the sheet thickness was 1.6 mm. **Table 1** shows the carbon content (mass%), carbon equivalent CE (mass%), and tensile strength (N • mm^{-2}) of the steel sheets tested. CE is the value obtained by Eq. (1). The elements in the equation indicate the content (mass%) in the steel.

$$CE = C + \frac{Si}{24} + \frac{Mn}{6} + \frac{Ni}{40} + \frac{Cr}{5} + \frac{Mo}{4} + \frac{V}{14} \text{ (mass\%)}$$

$$\text{..} \quad (1)$$

In Table 1, HT590 is a precipitation hardened steel, and HT780, HT980, and HT1180 are dual phase (DP) steels.

Figure 1 and **Table 2** show a schematic of the FSW tool and the FSW conditions, respectively. As the joint geometry, butt joints with a joint length of 250 mm were

Table 1 Carbon content, carbon equivalent, and tensile strength of steel sheets tested

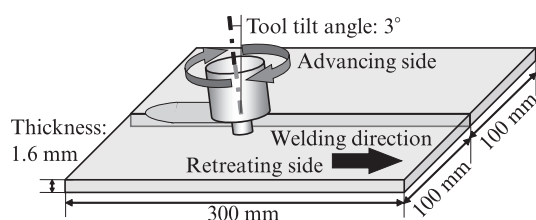| Mark	Carbon content (mass%)	Carbon equivalent, CE (mass%)	Tensile strength (N • mm^{-2})	Steel type
HT590	0.08	0.38	647	Precipitation hardened
HT780	0.05	0.46	795	Dual phase
HT980	0.09	0.61	1 015	Dual phase
HT1180	0.13	0.55	1 214	Dual phase

Fig. 1 Schematic of welding setup

Table 2 Welding conditions

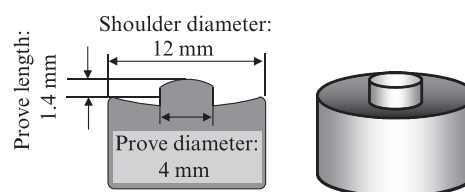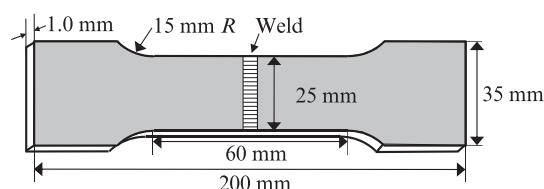| Tool rotation speed (min^{-1})	Travel speed (mm • min^{-1})	Tool tilt angle (°)
200–600	100–600	3

Fig. 2 Schematic of friction stir welding (FSW) tool

Fig. 3 Geometry of cross-weld tensile test specimen

used, and experiments were performed in the range of tool rotation speeds of 200–600 min^{-1} and travel speeds of 100–600 mm • min^{-1}. Welding was performed with 3° in leading tilt angle of FSW tool. At the two sides of the weld center line, the side where the tool revolution direction and the welding direction coincided was classified as the advancing side (AS), and the other side was classified as the retreating side (RS). **Figure 2** shows geometry of the tungsten carbide (WC) tool used in these experiments.

Cross-sectional observation of the obtained joints was performed at three positions 30 mm, 125 mm, and 220 mm from the start of welding to determine whether the joint contained defects. The joint microstructure was observed with an optical microscope after etching using picric acid saturated aqueous solution or nital as the etchant.

A cross-section joint hardness test and tensile test were performed to investigate the mechanical properties of the FSW joints. The joint hardness test was performed at the sheet center-of-thickness position with a micro Vickers hardness meter (load: 1.96 N). The tensile test was performed with test specimens of the geometry shown in **Fig. 3**. As the top and bottom sides were ground to obtain a smooth weld portion, the final thickness of the specimens was 1.0 mm.

2.2 Experimental Results and Discussion

Photo 1 shows the appearance of a representative FSW joint obtained in this experiment. Satisfactory surface quality could be obtained stably. **Photo 2** shows the transverse macrostructure (etched with picric acid solution) at the position 220 mm from the start of welding of HT780 under various conditions. Depending on the welding conditions, parts that were judged to be welding defects (incomplete consolidation) existed on the bottom side (shown by the open circles (○) in Photo 2).
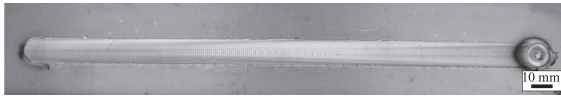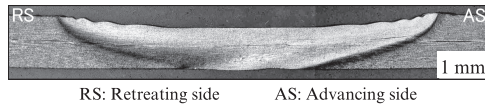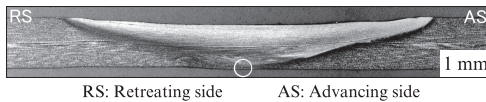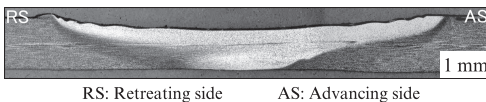
Photo 1 Appearance of representative weld produced by the experiment (HT780, Condition; Tool rotation speed: 200 min^{-1}-Travel speed: 200 mm・min^{-1})

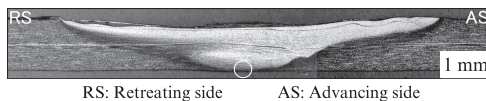RS: Retreating side   AS: Advancing side

(a) Condition; Tool rotation speed: 200 min^{-1}- Travel speed: 200 mm・min^{-1}

RS: Retreating side   AS: Advancing side

(b) Condition; Tool rotation speed: 200 min^{-1}- Travel speed: 400 mm・min^{-1}

RS: Retreating side   AS: Advancing side

(c) Condition; Tool rotation speed: 400 min^{-1}- Travel speed: 400 mm・min^{-1}
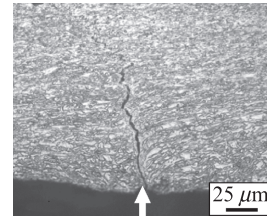

RS: Retreating side   AS: Advancing side

(d) Condition; Tool rotation speed: 400 min^{-1}- Travel speed: 600 mm・min^{-1}

Photo 2 Transverse macrostructures of welds of HT780 (Etched with picric acid solution)

(a) Condition; Tool rotation speed: 200 min^{-1}- Travel speed: 400 mm・min^{-1} (Photo 2(b))
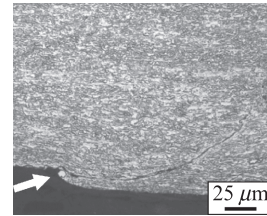
(b) Condition; Tool rotation speed: 400 min^{-1}- Travel speed: 600 mm・min^{-1} (Photo 2(d))

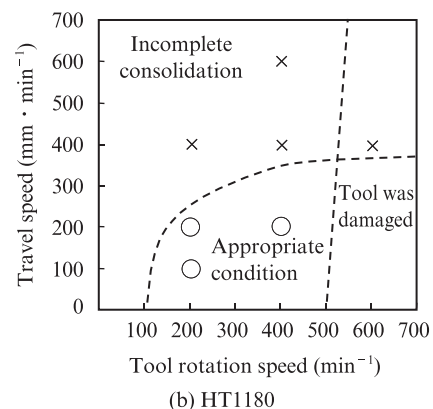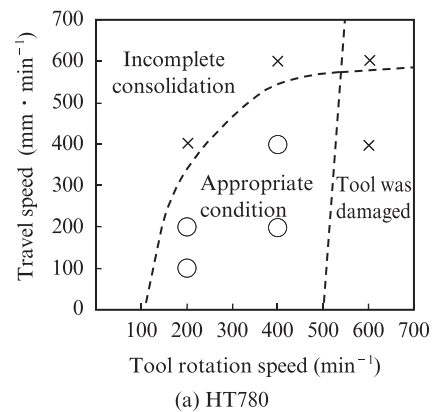Photo 3 Incomplete consolidation observed in transverse sections of welds of HT780

(a) HT780

(b) HT1180

Fig. 4 Appropriate welding parameter window

Enlarged views of those areas are shown in **Photo 3**. These joining defects are attributed to inadequate stirring on the bottom side, which left the original butting surfaces undissolved. Welding conditions under which defect-free welds could be confirmed by this type of cross-sectional observation were considered to represent the appropriate welding parameters for FSW. **Figure 4** shows the appropriate welding parameter windows as arranged for two steel grades, HT780 and HT1180. It may be noted that tool deformation occurred during welding at the tool rotation speed of 600 min^{-1}; therefore, this tool rotation speed was judged to be outside the appropriate welding parameter window, independent of cross-sectional observation.

As shown in Fig. 4(a), in the case of HT780, a satisfactory, defect-free joint as shown in Photo 2(a) was obtained at the tool rotation speed of 200 min^{-1} and travel speed of 200 mm・min^{-1}. However, at the travel speed of 400 min^{-1}, a defect was observed on the bottom side, as shown in Photo 2(b) and the enlargement in Photo 3(a). This is attributed to a decrease in heat input due to the increased travel speed, which resulted in a smaller stir zone (SZ). Comparing Photos 2(a) and (b), it can be understood that the size of the SZ decreased in (b), in which the travel speed was higher. In FSW of aluminum alloys, it is thought that the heat input decreases accompanying increases of the revolutionary pitch, which is defined by Eq. (2)[21].

(Revolutionary pitch (mm/r))

$$= \frac{\text{(Travel speed (mm} \cdot \text{min}^{-1}\text{))}}{\text{(Tool rotation speed (min}^{-1}\text{))}} \quad \cdots\cdots\cdots\cdots \quad (2)$$

This thinking is considered to be the same in FSW of ferrous materials. Thus, it is presumed that heat input decreases as the revolutionary pitch increases due to increased travel speed.

On the other hand, in the case of the tool rotation speed of 400 min^{-1}, no defects were observed, as shown in Photo 2(c), even at the travel speed of 400 mm $\cdot$ min^{-1}. However, a defect was observed when the travel speed was increased to 600 mm $\cdot$ min^{-1}, as shown in Photo 2(d) and Photo 3(b). In this case, welding is considered to be possible at higher speeds because the revolutionary pitch decreases due to the increased tool rotation speed, which means the heat input increases. However, the tool damage at the tool rotation speed of 600 min^{-1} is considered to be the result of softening of the WC tool due to the temperature rise caused by excessive frictional heating at the interface between the tool and steel sheet surface. From this, it can be said that an excessive increase of the tool rotation speed leads to tool damage.

In the case of HT1180, as shown in Fig. 4(b), a defect was confirmed under the conditions of a tool rotation speed of 400 min^{-1} and travel speed of 400 mm $\cdot$ min^{-1}. Thus, the appropriate welding parameter window is narrower in comparison with HT780. This is estimated to be the result of shallower insertion of the tool tip probe due to increased counteraction to tool pressure from the area around the weld zone as the strength of the steel sheet increases. Shallower insertion decreases the size of the SZ, and consequently, defects occur more easily under the same welding conditions.

As described above, although the appropriate parameter window is narrower with HT1180 in comparison with HT780, these experiments confirmed that an appropriate parameter window, within which it is possible to obtain satisfactory, defect-free welds, exists for both of these steel sheets.

Photo 4 shows the transverse macrostructure of a weld of HT780 (etched with nital) when welding was performed under conditions of a rotation speed of 200 min^{-1} and travel speed of 200 mm $\cdot$ min^{-1}. Friction
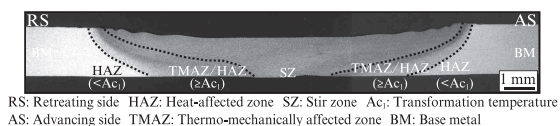
stir welds are generally classified into three regions, namely, the SZ, the thermo-mechanically affected zone (TMAZ), and the heat affected zone (HAZ). However, based on the distinctive changes in the microstructure in the transverse macrostructure shown in Photo 4, this weld was classified into the following three regions: SZ, TMAZ/HAZ$>$Ac$_1$ (thermo-mechanically affected zone/ heat affected zone heated to above the Ac$_1$ point, which is the transformation point ($\alpha+\theta \rightarrow \alpha+\gamma$) when steel is heated), and HAZ$<$Ac$_1$ (heat affected zone heated to below the Ac$_1$ point). The microstructures of these regions are shown in **Photo 5**. Because HT780 is a DP steel, the base metal (BM) has a mixed microstructure of ferrite and martensite, as shown in Photo 5(d). On the other hand, the SZ differs greatly from the BM, in that
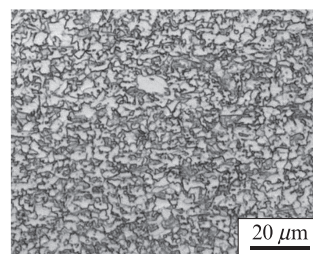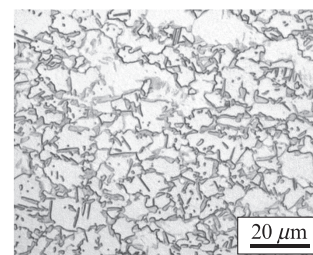

(a) SZ (Stir zone)
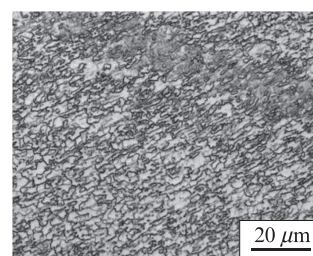
(b) TMAZ/HAZ$\geqq$Ac$_1$
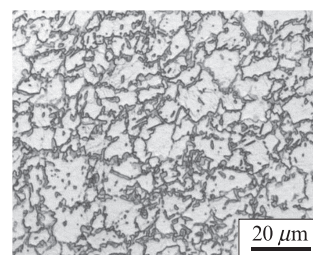
(c) HAZ$<$Ac$_1$

(d) BM (Base metal)

Photo 5 Microstructures in SZ of welds of HT780, Etched with natal (Condition: 200 min^{-1}-200 mm $\cdot$ min^{-1})

RS: Retreating side HAZ: Heat-affected zone SZ: Stir zone Ac$_1$: Transformation temperature
AS: Advancing side TMAZ: Thermo-mechanically affected zone BM: Base metal

Photo 4 Transverse macrostructure of weld of HT780 (Etched with natal, Condition: 200 min^{-1}-200 mm $\cdot$ min^{-1})

the SZ has an extremely fine mixed microstructure that includes ferrite, bainite, and martensite. Accordingly, when the SZ is heated to above the Ac_1 point during welding, it is considered that partial or complete reverse transformation to austenite occurs, and the microstructure then transforms once again to ferrite, bainite, and martensite during cooling after experiencing large strain due to friction stirring. Furthermore, at the outer side of the SZ, a TMAZ/HAZ$\geqq$$Ac_1$ region exists, where the TMAZ/HAZ is heated to above the Ac_1 point and is partially affected by strain. This region, as shown in Photo 5(b), exhibits a microstructure similar to that of the SZ, and it is considered that the heat cycle during welding approximates that of the SZ. At the outer side of this TMAZ/HAZ$\geqq$$Ac_1$ region, a HAZ$<$$Ac_1$ exists, where the material is heated to below the Ac_1 point. Since this region does not undergo reverse transformation to austenite during welding, it displays a microstructure, as shown in Photo 5(c) similar to that of the BM; however, hardness decreases remarkably in this region because the martensite of the BM is affected by tempering.

Figure 5 shows the hardness profile of the transverse section of a weld of HT780 after welding at the tool rotation speed of 200 min^{-1} and travel speed of 200 mm $\cdot$ min^{-1}. The hardness of the SZ is around HV255 and is approximately the same as that of the BM. In contrast, softening could be seen near the boundary between TMAZ/HAZ$\geqq$$Ac_1$ and the HAZ$<$$Ac_1$. This is considered to be due to tempering of the martensite phase in the BM.
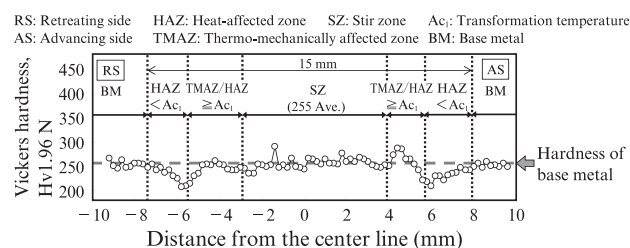
Figure 6 shows the hardness profile of a joint of

HT1180 that was welded under the conditions of tool rotation speed and travel speed of 200 min^{-1} and 200 mm $\cdot$ min^{-1}, respectively. While the hardness around the center of the SZ increased to more than that of the BM, remarkable softening in comparison with the BM could be seen in the region from the TMAZ/HAZ$\geqq$$Ac_1$ to the HAZ$<$$Ac_1$. Although HT1180 is also a DP steel, because its strength is higher than that of HT780, the ratio of martensite in the BM is higher. Accordingly, softening is considered to be greater in HT1180 because tempering of the BM martensite by heating below the Ac_1 point is more significant.

Figure 7 shows the relationship between the tensile strength of the base metal and welded joints obtained with HT590, HT780, HT980, and HT1180 when welding was performed under the conditions of tool rotation speed of 200 min^{-1} and travel speed of 200 mm $\cdot$ min^{-1}. The HT590 joint fractured in the BM, and the tensile strength of the joint was similar to that of the BM. The fractures of the joints of HT780, HT980, and HT1180 all occurred in the HAZ, and joint efficiency, as defined by Eq. (3), was HT780=96%, HT980=95%, and HT1180=84%.

$$\text{(Joint efficiency (\%))}$$
$$= \frac{\text{(Joint tensile strength (N} \cdot \text{mm}^{-2}))}{\text{(Base metal tensile strength (N} \cdot \text{mm}^{-2}))} \times 100$$
$$\cdots\cdots\cdots\cdots\cdots\cdots\cdots\cdots\cdots\cdots\cdots\cdots\cdots (3)$$

These results confirmed that the tensile strength of joints produced by FSW is roughly the same as that of the base metal in high tensile strength steel sheets up to 980 N $\cdot$ mm^{-2} in spite of softening of the HAZ.

RS: Retreating side   HAZ: Heat-affected zone   SZ: Stir zone Ac_1: Transformation temperature
AS: Advancing side   TMAZ: Thermo-mechanically affected zone   BM: Base metal

Fig. 5   Hardness profiles in transverse sections of welds of HT780 (Condition: 200 min^{-1}-200 mm $\cdot$ min^{-1})
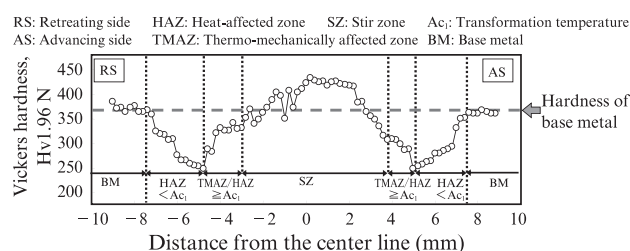

RS: Retreating side   HAZ: Heat-affected zone   SZ: Stir zone Ac_1: Transformation temperature
AS: Advancing side   TMAZ: Thermo-mechanically affected zone   BM: Base metal

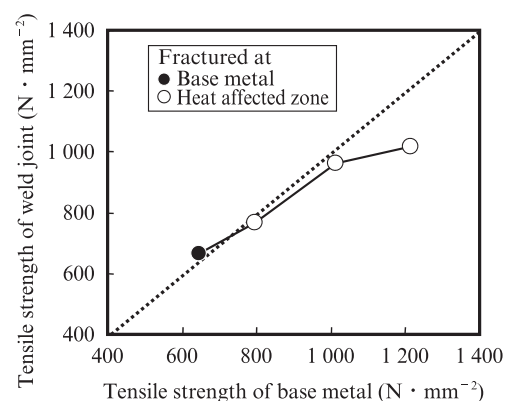Fig. 6   Hardness profile in transverse section of weld of HT1180 (Condition: 200 min^{-1}-200 mm $\cdot$ min^{-1})

Fig. 7   Relationship between tensile strengths of base metals and weld joints(Condition; Tool rotation speed: 200 min^{-1}-Travel speed: 200 mm $\cdot$ min^{-1})

3. FSW of Structural Steel Plates

3.1 Experimental Method

Welding experiments were performed by using structural steel plates with a plate thickness of 12 mm and tensile strength of 400 N • mm^{-2} class. **Table 3** shows the chemical composition of the tested steel plate. **Table 4** shows the welding conditions. Butt-welded joints with a length of 450 mm were prepared. A polycrystalline cubic boron nitride (PCBN) tool of the shape shown in **Photo 6** was used as the FSW tool.

Cross-sectional observation was performed at three locations 50, 225, and 400 mm from the start of welding to determine whether the joints contained defects. The microstructures of the stir zone (SZ) and the thermomechanically affected zone/heat affected zone (TMAZ/HAZ) were etched with a picric acid saturated aqueous solution or nital and observed with an optical microscope. Weld hardness was evaluated by testing the plate center-of-thickness position with a micro Vickers hard-

ness meter (load: 4.9 N). A tensile test was performed with a test specimen geometry conforming to ISO 4136 (JIS Z 3121, JIS: Japanese Industrial Standards), as shown in **Fig. 8**. Samples of two thicknesses were prepared, one with the original plate thickness and the other with a plate thickness of 10 mm by grinding 1.0 mm each from the top and bottom sides in order to smoothen the weld portion. The Charpy impact test was performed by taking a sample of a shape conforming to ISO/DIS 148-1 (JIS Z 2242) from the center-of-thickness position, and making notches at positions 1 mm and 3 mm to the retreating side (RS) from the center of the weld line (these notches are denoted by −1 mm, −3 mm) and 1 mm and 3 mm to the advancing side (AS) (denoted by 1 mm, 3 mm).

3.2 Experimental Results and Discussion

Photo 7 shows the results of observation of the cross-sectional macrostructure at the position 225 mm from the start of welding. A sound joint was obtained, with no incomplete consolidation or other defects in the weld. As shown in Photo 7, the weld was classified into three regions, i.e., the stir zone (SZ), thermo-mechanically affected zone (TMAZ), and the heat affected zone (HAZ). **Figure 9** shows the joint hardness profile. The hardness of the SZ is higher than that of the BM, and within the SZ, the hardness of the AS is higher than that of the RS. This variation of hardness within the SZ is considered to be caused by the microstructures of the

Table 3   Chemical composition of tested steel plate

(mass%)

Chemical composition					
C	Si	Mn	P	S	CE
0.13	0.2	1.0	0.01	0.002	0.31

Table 4   Welding condition

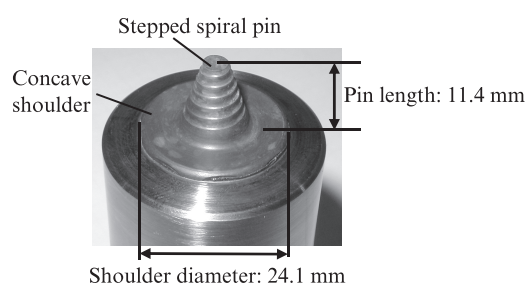| Tool rotation speed (min^{-1})	Travel speed (mm • min^{-1})	Tool tilt angle (°)
450	51.0	3.5

Photo 6   Appearance of friction stir welding (FSW) tool

Fig. 8   Geometry of cross-weld tensile test specimen (Complying with ISO 4136 (JIS Z 3121))
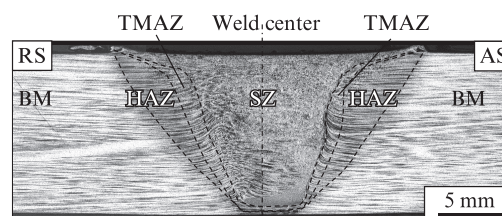
RS: Retreating side   HAZ: Heat-affected zone   SZ: Stir zone
AS: Advancing side   TMAZ: Thermo-mechanically affected zone
BM: Base metal

Photo 7   Transverse macrostructure of weld of the steel plate tested (Etched with picric acid solution)
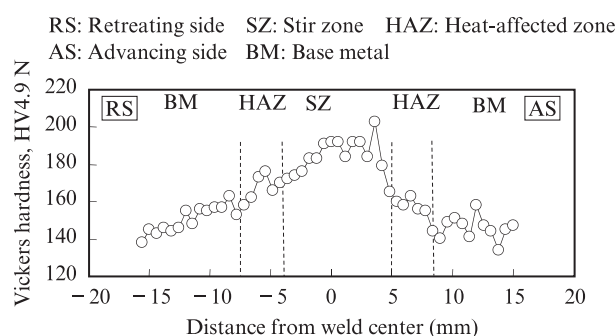

Fig. 9   Hardness profile in transverse section of weld

Table 5   Results of cross-weld tensile test

Thickness of sample	Tensile strength (N · mm^{-2})	Region of fracture	
12 mm (As welded)	470	Base metal	
10 mm (Reduced)	479	Base metal	

SZ: Stir zone   BM: Base metal
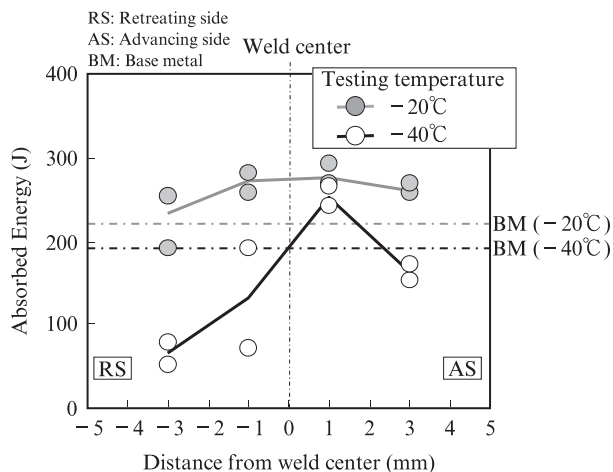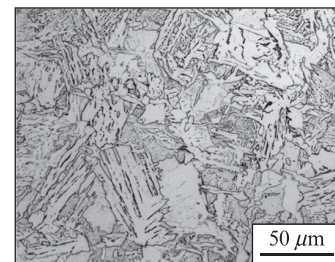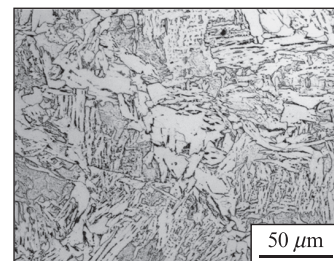

Fig. 10   Charpy toughness variation across the weld

(a) −3 mm from weld center

(b) −1 mm from weld center

(c) 1 mm from weld center

(d) 3 mm from weld center

Photo 8   Microstructures of stir zone (SZ) corresponding to the notch locations of tested Charpy specimens

respective positions. **Table 5** shows the results of the cross-weld tensile test. Fracture occurred in the BM in both the specimen with the original thickness and the specimen with the thickness reduced to 10 mm.
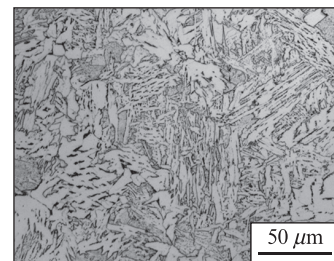
Figure 10 shows the results of the Charpy impact test with the notch positions of −3 mm, −1 mm (RS) and 1 mm, 3 mm (AS). The average absorbed energy of the BM at the respective test temperatures of −40°C and −20°C is shown by the broken lines in the figure. At the test temperature of −20°C, higher absorbed energy than that of the BM was obtained at all notch positions, indicating excellent toughness. On the other hand, at the test temperature of −40°C, which is a severer test condition, the absorbed energy on the AS was on the same level as that of the BM, but the values of the RS were lower. **Photo 8** shows the microstructures at the positions corresponding to the four notches described above. The main components of the microstructure at the positions of −3 mm and −1 mm (RS) were the grain boundary ferrites including grain boundary polygonal ferrite (GPF) and ferrite side plate (FSP), On the other hand, at the positions of 1 mm and 3 mm (AS), intragranular acicular ferrite (IAF) that evolved from inside the grains could be seen in addition to grain boundary ferrites. From the above, at the test temperature of −20°C, satisfactory toughness could be obtained at all notch positions in the SZ, but at −40°C, Charpy absorbed energy showed vari-
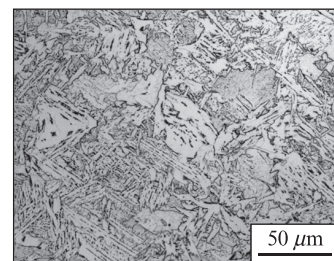
ations within the SZ. This is conceivably attributable to a change in the ductile-brittle transition temperature due to inhomogeneous evolution of the microstructure in the SZ.

4. Conclusions

Friction stir welding (FSW) was performed using advanced high strength steel sheets of 4 tensile strength grades from 590 to 1 180 N·mm^{-2} and thickness of 1.6 mm. The following conclusions were obtained.

(1) The appropriate welding parameter windows for HT780 and HT1180 were verified. The results revealed that a narrower parameter window exists for HT1180 in comparison with HT780.

(2) From the microstructure and hardness profile of the weld of the HT780 joint, the microstructure changes distinctively in three regions, namely, the stir zone (SZ), which is heated to above the Ac_1 point, the thermo-mechanically affected zone/heat affected zone above the Ac_1 point (TMAZ/HAZ $>$ Ac_1) surrounding the SZ, and the heat affected zone below the point (HAZ $<$ Ac_1).

(3) In FSW of high tensile strength steel sheets, it was found that joints of approximately the same strength as the base metal can be obtained with sheets up to the tensile strength grade of 980 N·mm^{-2}, and the possibility of improving joint strength by controlling the welding parameters was also shown in sheets exceeding 980 N·mm^{-2}.

Friction stir welding (FSW) was also performed using structural steel plates of tensile strength grade 980 N·mm^{-2} and thickness of 12 mm. The conclusions are summarized as follows.

(4) Sound, defect-free welds could be obtained with plates having a thickness of 12 mm.

(5) In the cross-weld tensile test, fracture occurred in the base metal, indicating that strength on the same level as the base metal was obtained.

(6) At the test temperature of $-20°C$, satisfactory toughness was obtained uniformly within the SZ, whereas at $-40°C$, Charpy absorbed energy varied within the SZ. This is conceivably attributable to a change in the ductile-brittle transition temperature due to inhomogeneous microstructure evolution.

References

1) Thomas, W. M.; Nicholas, E. D.; Needham, J. C.; Murch, M. G.; Temple-Smith, P.; Dawes, C. J. International Patent Application No. PCT/GB92/02203.
2) Dawes, C. J.; Thomas, W. M. Weld. J. 1996-03, vol. 75, p. 41–45.
3) Park, S. H. C.; Sato, Y. S.; Kokawa, H. Scripta Mater. 2003, vol. 49, p. 161–166.
4) Fujii, H.; Ueji, R.; Takada, Y.; Kitahara, H.; Tsuji, N.; Nakata, K.; Nogi, K. Mater. Trans. 2006, vol. 47, no. 1, p. 239–242.
5) Lienert, T. J.; Stellwag, W. L.; Grimmett, B. B.; Warke, R. W. Weld. J. 2003-01, vol. 82, p. 1s–9s.
6) Reynolds, A. P.; Tang, W.; Posada, M.; DeLoach, J. Sci. Technol. Weld. Join. 2003, vol. 8, no. 6, p. 455–460.
7) Konkol, P. J.; Mathers, C. J. A.; Johnson, R.; Pickens, J. R. J. Ship Prod. 2003-08, vol. 19, no. 3, p. 159–164.
8) Ueji, R.; Fujii, H.; Cui, L.; Nishioka, A.; Kunishige, K.; Nogi, K. Mater. Sci. Eng. A. 2006, vol. 423, p. 324–330.
9) Fujii, H.; Cui, L.; Tsuji, N.; Maeda, M.; Nakata, K.; Nogi, K. Mater. Sci. Eng. A. 2006, vol. 429, p. 50–57.
10) Cui, L.; Fujii, H.; Tsuji, N.; Nakata, K.; Nogi, K.; Ikeda, R.; Matsushita, M. ISIJ Int. 2007, vol. 47, no. 2, p. 299–306.
11) Cui, L.; Fujii, H.; Tsuji, N.; Nogi, K. Scripta Mater. 2007, vol. 56, p. 637–640.
12) Ayer, R.; Fairchild, D. P.; Ford, S. J.; Nissley, N. E.; Jin, H. W.; Ozekcin, A. et al. Proc. of 7th Int. Friction Stir Welding Symp. TWI, Cambridge, UK, 2008.
13) Matsushita, M.; Kitani, Y.; Ikeda, R.; Ono, M.; Fujii, H.; Chung, Y. D. Quarterly Journal of the Japan Welding Society. 2009, vol. 27, no. 4, p. 360–370.
14) Matsushita, M.; Kitani, Y.; Ikeda, R.; Ono, M.; Fujii, H.; Chung, Y. D. Sci. Technol. Weld. Join. 2011, vol. 16, no. 2, p. 181–187.
15) Matsushita, M.; Kitani, Y.; Ikeda, R.; Fujii, H. ISIJ Int. 2012, vol. 52, no. 7, p. 1335–1341.
16) Reynolds, A. P.; Tang, W.; Gnaupel-Herold, T.; Prask, H. Scripta Mater. 2003, vol. 48, p. 1289–1294.
17) Park, S. H. C.; Sato, Y. S.; Kokawa, H.; Okamoto, K.; Hirano, S.; Inagaki, M. Scripta Mater. 2003, vol. 49, p. 1175–1180.
18) Zhu, X. K.; Chao, Y. J. J. Mater. Process. Technol. 2004, vol. 146, p. 263–272.
19) Sato, Y. S.; Nelson, T. W.; Sterling, C. J.; Steel, R. J.; Pettersson, C.-O. Mater. Sci. Eng. A. 2005, vol. 397, p. 376–384.
20) Sato, Y. S.; Nelson, T. W.; Sterling, C. J. Acta Mater. 2005, vol. 53, p. 637–645.
21) Liu, H. J.; Fujii, H.; Maeda, M.; Nogi, K. J. Mater. Process. Technol. 2003, vol. 142, p. 692–696.